CrossMark

Effect of orifice shape on bubble formation mechanism

Pedram Hanafizadeh · Amirmohammad Sattari · Seyed Erfan Hosseini-Doost ·
Arash G. Nouri · Mehdi Ashjaee

Abstract The effect of orifice shape on the mechanism of bubble formation in gas–liquid two-phase flow is investigated experimentally with three different orifice geometries regarding a circle, a square, and a triangle with same cross-sectional areas. The liquid and gas phases are purified water at 20 °C and air at room temperature, respectively. Gas is injected at the rate of 50–1200 mlph into a stagnant pool of liquid in distances of 5, 10, and 15 cm below the liquid surface. The position, velocity, and acceleration of bubbles are measured at bubbles' centers of mass (CM) and the effects of these parameters on the bubble volume are investigated. Moreover, the forces acting on a bubble are balanced and the effects of geometry and gas flow rate on each force are presented. In addition, the changes of the acting forces versus time are plotted and discussed for a specific condition. Results show the bubbles formed with the square and circular orifice cross-sectional areas have the most and least volumes at detachment, respectively.

1 Introduction

The dynamic of bubble formation has a major role in diverse applications related to scattering of gas bubbles in liquids, including chemical reactors, water treatment instruments, and a variety of chemical plants and processes such as perforated plate columns and fluidized beds. It can also be used to imitate bubble departure in nucleate boiling. This phenomenon is affected by different parameters such as diameter of injection, geometry of injection, gas flow rate, liquid and gas physical properties, height of the liquid column, and wettability. Influence of some mentioned parameters has been analyzed in literature and is summarized briefly below.

1.1 Gas flow rate

Most of the researches done in the field of bubble formation process include the effect of gas flow rate on the bubble characteristics. Davidson and Schuler [1] investigated the formation of bubbles with an orifice in a viscous liquid flow. They found that at any particular

P. Hanafizadeh (✉) · A. Sattari · S. E. Hosseini-Doost ·
M. Ashjaee
Center of Excellence in Design and Optimization of
Energy Systems, School of Mechanical Engineering,
College of Engineering, University of Tehran,
P. O. Box: 11155, Tehran, Iran
e-mail: hanafizadeh@ut.ac.ir

A. G. Nouri
Department of Mechanical Engineering and Materials
Science, University of Pittsburgh,
P. O. Box: 15261, Pittsburgh, PA, USA

viscosity, the frequency of bubble formation is almost constant, and the changes in gas flow rate exclusively change the volume of individual bubbles. Satyanarayan et al. [2] also studied the bubble formation process under constant pressure conditions. They inferred that for large orifices, the bubble volume remains constant for a range of flow rates and for flow rates more than a determined critical value, bubble volume increases with increase in flow rate. Sada et al. [3] had a study on bubble formation in flowing liquids. They found that the size of bubbles formed in a flowing liquid is decreased by decreasing the gas flow rate. In another research, Oguz and Prosperetti [4] investigated several aspects of the growth and departure of bubbles from a submerged needle. They inferred that two different growth regimes exist according to whether the gas flow rate into the bubble is smaller or greater than a critical value. In addition, they concluded that bubbles growing in a flowing liquid parallel to the needle might detach with a considerably smaller radius than in a quiescent liquid. Takagi et al. [5] obtained the drag coefficient (C_D) of a gas bubble in an axisymmetric shear flow as a function of Reynolds (Re) and Weber (We) numbers. Vafaei et al. [6] studied bubble growth rate from stainless steel substrate and needle nozzles. They found that when a bubble forms at the top of the needle nozzle, the nominal and the average gas flow rates would be slightly different.

1.2 Physical properties of liquid phase

Many experimental investigations have been done on the influence of different physical properties like surface tension of liquid phase, dynamic viscosity, density, and height of the liquid column on bubble characteristics. Ramakrishnan et al. [7] studied the bubble formation mechanism under constant flow conditions. They detected that in the case of low viscous liquids, the surface tension force is effective at low flow rates but its importance continuously decreases as the flow rate increases. Ramakrishnan and Kumar [8] investigated the influence of liquid density on bubble volume. They observed that when the flow rate and viscosity are small, the bubble volume decreases with increasing the liquid density. When the flow rate is large and the viscosity is small, for small orifice diameters, the bubble volume is independent of liquid density. Moreover, as the flow

rate is increased, viscous drag and inertial force increase while that of the surface tension term remains constant. Therefore, the effect of other factors becomes more important and the relative contribution of the surface tension force to the total bubble volume becomes less. Bubble formation in quiescent liquids under constant flow conditions were studied by Gaddis and Vogelpohl [9]. They found that when the force due to gas momentum exceeds the surface tension force, the surface tension won't be able to form spherical or quasi-spherical bubbles. Terasaka and Tsuge [10] also had an experimental study on bubble formation process under constant flow conditions. They deduced that bubble volume increases by increasing the dynamic viscosity. Hao and Prosperetti [11] worked on the effect of viscosity on the spherical stability of oscillating gas bubbles. A numerical method for the solution of the pertinent equations was presented and a good agreement between theory and numerical data was found. Jamialahmadi et al. [12] also studied the same. They concluded at low gas flow rates the bubble size is almost independent of liquid viscosity while at high gas flow rates, the bubble size increases considerably as the liquid viscosity increases. Liquid height is another parameter that was investigated by Das et al. [13]. They studied the bubble formation process at submerged orifices and found that the bubble frequency decreases by increasing the liquid height.

1.3 Orifice and needle diameter

Orifice diameter is one of the important affecting parameters in bubble formation process. One of the first studies about the influence of orifice diameter on bubble formation was conducted by Fritz [14]. He presented one of the first correlation of maximum radius of bubble in term of orifice radius. Terasaka and Tsuge [15] experimentally investigated this process on a single orifice in non-Newtonian liquids. They concluded the volume of a bubble increases with decreasing the orifice diameter at relatively low gas flow rates, while the orifice diameter doesn't have any influence on bubble volume at high gas flow rates. Badam et al. [16] also did experimental investigations on the regimes in bubble formation process on submerged orifices under constant flow conditions. They observed that the bubble formation time-period increases with increasing the orifice diameter at any amount of gas flow rate. Fan et al. [17] used three

circular orifices with diameters of 1, 1.5, and 2 mm and concluded that by increasing orifice diameter, volume of bubbles increases too. In another research, three orifice diameters of 0.58, 1.05, and 1.6 mm were utilized by Bari and Robinson [18] in order to investigate the effect of orifice diameter. They concluded that bubbles generated from smaller orifices had lower volumes and departure times, and remained more spherical. Hanafizadeh et al. [19] investigated the effect of needle diameter on the bubble frequency and the bubble volume at detachment. They found that the volume of the detached bubble increases by increasing the needle diameter and dispersed phase (gas) flow rates.

1.4 Contact angle

Contact angle is a significant variable which is strongly effective on bubble parameters. Some researchers have investigated the influence of this parameter. Kulkarni and Joshi [20] presented two types of surface tension force (dynamic and static) acting on a bubble. In the initial part of bubble growth phase in their work, the surface tension was dynamic and the contact angle with the orifice surface was changing continuously, while in the next part, the bubbles reached a constant contact angle and were approaching to a static surface tension. In the latter part, the surface tension determined the orientation time/growth time for bubbles. Corchero et al. [21] studied the effect of wetting conditions and flow rate on bubble formation on orifices submerged in water. Both hydrophilic and hydrophobic materials used in this study were utilized to cover a range of static contact angles ($68° \leq \theta_0 \leq 123°$). It was shown that by properly plotting the scaled bubble volume at detachment versus a scaled volumetric gas flow rate, the data from different static contact angles and orifice radii could be reduced to a single bubble volume/flow rate relation. Furthermore, they concluded the maximum bubble volume was attained in the quasi-static regime when the static contact angle was $\theta_0 = 90°$. Vafaei and Wen [22] studied the bubble formation mechanism in a submerged micro nozzle and concluded that the variations of instantaneous contact angles were strongly dependent on the bubble volume but weak functions of flow rates. In another work, Di Bari and Robinson [18] did an experimental study on bubble growing phenomenon on bubbles generated from a submerged orifice. They found that the decrease in contact angle was largely due to a decrease in the ratio of buoyancy force over the orifice size. Finally, Hanafizadeh et al. [19] evaluated the effects of gas properties on the mechanism of bubble formation. Results showed that the contact angle increased by increasing the gas flow rate.

Despite extensive researches on bubble formation process, to the authors' knowledge, there is not any experimental study on the effect of the geometry of injection on major parameters that affect the bubble formation mechanism. It has been demonstrated that the contact line has a significant impact on the contact angle line hysteresis [23]. The main purpose of this research is to evaluate the effect of circular, square, and triangular cross-sectional geometries of the air injecting needle on major parameters of the bubble such as volume, frequency, contact angle, etc. in constant flow conditions during its formation. One of the major conditions that influences bubble formation process is the velocity of the injection. So, this parameter is fixed for the needles by considering the same cross-sectional area for different geometries and same flow rate. First, dynamic of bubble formation contains the CM position, velocity, acceleration, bubble equivalent diameter, and contact angle and effect of needle geometry are investigated. Next, by balancing the effective forces on bubbles, the effects of flow rate and shape of the needle on the magnitude and the contribution of each force are investigated. Also, this force balancing is verified during the bubble formation process by computing acting forces and summation of the forces at different times. Finally, the effects of geometry, gas flow rate, and liquid height are perused on bubble formation frequency, bubble equivalent diameter, necking time, and bubble height.

2 Experimental apparatus

The experimental setup used in this work includes a syringe pump, a water container, air injecting needles with circular, square and triangular cross-sectional areas, and a high-speed camera. For optical and photographic observations, the square column made from polymethyl methacrylate (PMMA) with dimensions 100 mm × 100 mm × 300 mm and open to the atmosphere at the top was used. The height of the liquid is 5, 10, and 15 cm above the needle. In order to

inject gas into the liquid phase under constant flow condition, an automatic controlled syringe pump (AMPall SP8800) was utilized. The syringe was filled with gas and the flow rate range is between 50 and 1200 mlph.

The innovative part of this work is the experimental investigation of the effect of square and triangular needles on the mechanism of bubble formation. To achieve this aim, two square and triangular cross-sectional needles were built from steel material using wire cut method in addition to a standard G14 circular needle. Because of structural constraints, the inner edges of the needles were built with a 0.3 mm fillet and with the minimum of 0.5 mm thickness. These needles have the same height which is equal to 40 mm. The cross-sections of the needles are shown in Fig. 1. Also, a 3D view of needles can be seen in Fig. 2.

The range of the operating conditions used in the studies is listed in Table 1.

A high-speed camera is utilized to record the bubble formation process. The simulation of lighting system with DIALux 4.11 shows applying an 800 W halogen lamp provides appropriate illumination for high-speed photography (the lamp is placed just in front of the high-speed camera as shown in Fig. 3). The high-speed mode, (1200 fps) with a resolution of 336 × 96 pixels, is selected for taking images. All captured images are analyzed with an image processing (IP) computer code in order to obtain the required bubble properties including the bubble volume (equivalent diameter), the frequency of formation, necking time, contact angle, and bubble height. Schematic of the experimental setup is shown in Fig. 3.

When we use the experimental measurements, there are uncertainties due to measurement limitations. In this study, the uncertainties of measured data are shown in Table 2. The precision of the major parameters is reported in this table based on the accuracy of the measuring instruments. The error bars in the following figures are generated based on these uncertainties.

As seen in Table 2, images have an uncertainty due to calibration scale. This uncertainty makes errors in finding the edge of bubbles and other parameters like the height and width of the bubble. In order to consider repeatability of the tests, all experiments are done triple times and the average values of different experiments are utilized.

3 Image processing method

Captured photos by the camera require a filtering series. As shown in Fig. 4a, the first filter is "rg-b2gray" which converts the actual color image RBG to a gray-scaled intensity image. As shown in Fig. 4b, the second filter is "im2bw" which converts the gray-scaled image to a binary image.

After using the filters, the code finds the edges of bubbles as shown in Fig. 4c. The volume of the bubble is calculated by revolving the bubble boundary in Fig. 4d around its vertical axis. It is assumed that the bubbles are axisymmetric since they begin to form on the orifice surface. For justification of this claim, at the same time, a sequence of bubble from axial and transversal directions for triangular orifice at 1000 mlph has been captured using a same camera and the volumes are compared (Fig. 5). The bubble volumes which are resulted from axisymmetric assumption for axial and transversal directions have
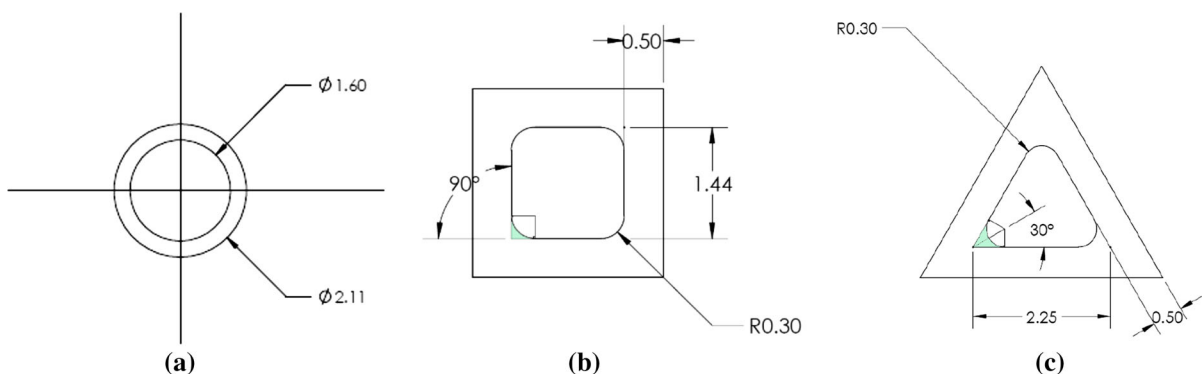

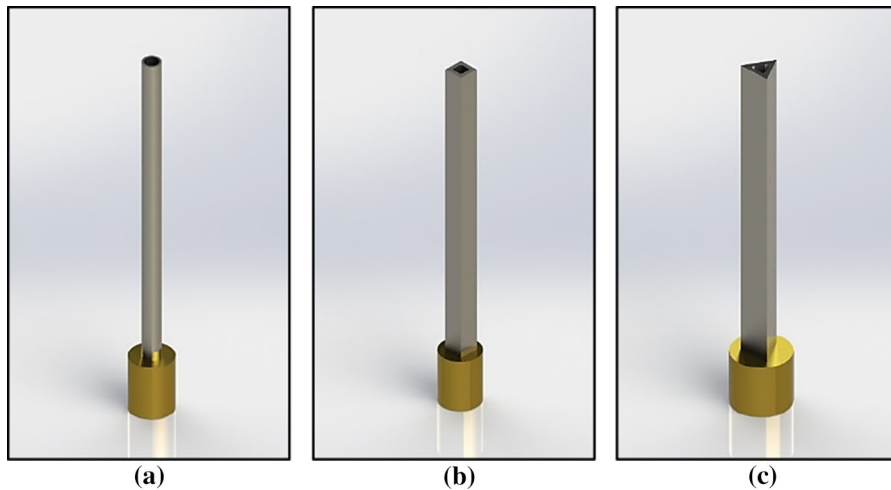Fig. 1 a Circular b square and c triangular cross-sectional areas of the air injecting needle

Fig. 2 Three-dimensional view of **a** circular **b** square and **c** triangular needles

Table 1 Range of operating conditions

Operating parameter	Parameter value
Flow rate	50–1200 mlph
Liquid height above the needle	50, 100, and 150 mm
Liquid viscosity	0.001 Pa s
Air viscosity	0.00018 Pa s
Surface tension	72.5×10^{-3} N m^{-1}
Liquid density	997.05 kg m^{-3}
Air density	1.15 kg m^{-3}

about 5% differences. This confirms that the assumption of the axisymmetric bubble is almost true. Because as mentioned before, the bubbles begin to form on the orifice surface and although the shape has an influence on bubbles especially at corners of the orifice, there is no significant difference between the shape of the bubble in axial and transversal directions. As a matter of fact, we can suppose that the rim of the bubble is almost circumscribed circle of the triangle. In fact, this is the key difference between circular and other shapes of the orifice with the same cross-sectional area.

By finding the edge of the bubbles the height of them, H, and the largest distance between left and right edges of the bubbles, W_{max}, are determined in order to calculate the projection area, A_{pro}, which will be used in calculating of drag force. The contact angle of a bubble is found by ellipse fitting method, which provides high accuracy for a wide range of angles.

In order to compute the frequency of bubbles, a line is defined over the orifice needle which counts the bubbles as they cross it. Then, the frequency is dividing the number of bubbles to the elapsed time from the first to the last bubble. We compute the CM of bubbles in dynamic analysis with

$$y_{CM} = \int_0^H m_i dy_i / M,, \tag{1}$$

where y_{CM} is the position of bubble CM, m_i and dy_i are the mass and height of the ith element, respectively, and M is the total mass of the bubble. By assuming that the density of air is constant all over the bubble, Eq. (1) can be written as follows:

$$y_{CM} = \int_0^H v_i dy_i / V, \tag{2}$$

where v_i and V are the volume of the ith element and total volume of the bubble, respectively. A sequence of CM position of a bubble is shown in Fig. 6. For more details of IP method see Ref. [24].

4 Force balancing

A theoretical model is used to balance the effective forces on bubbles. The underlying assumptions are as follows:
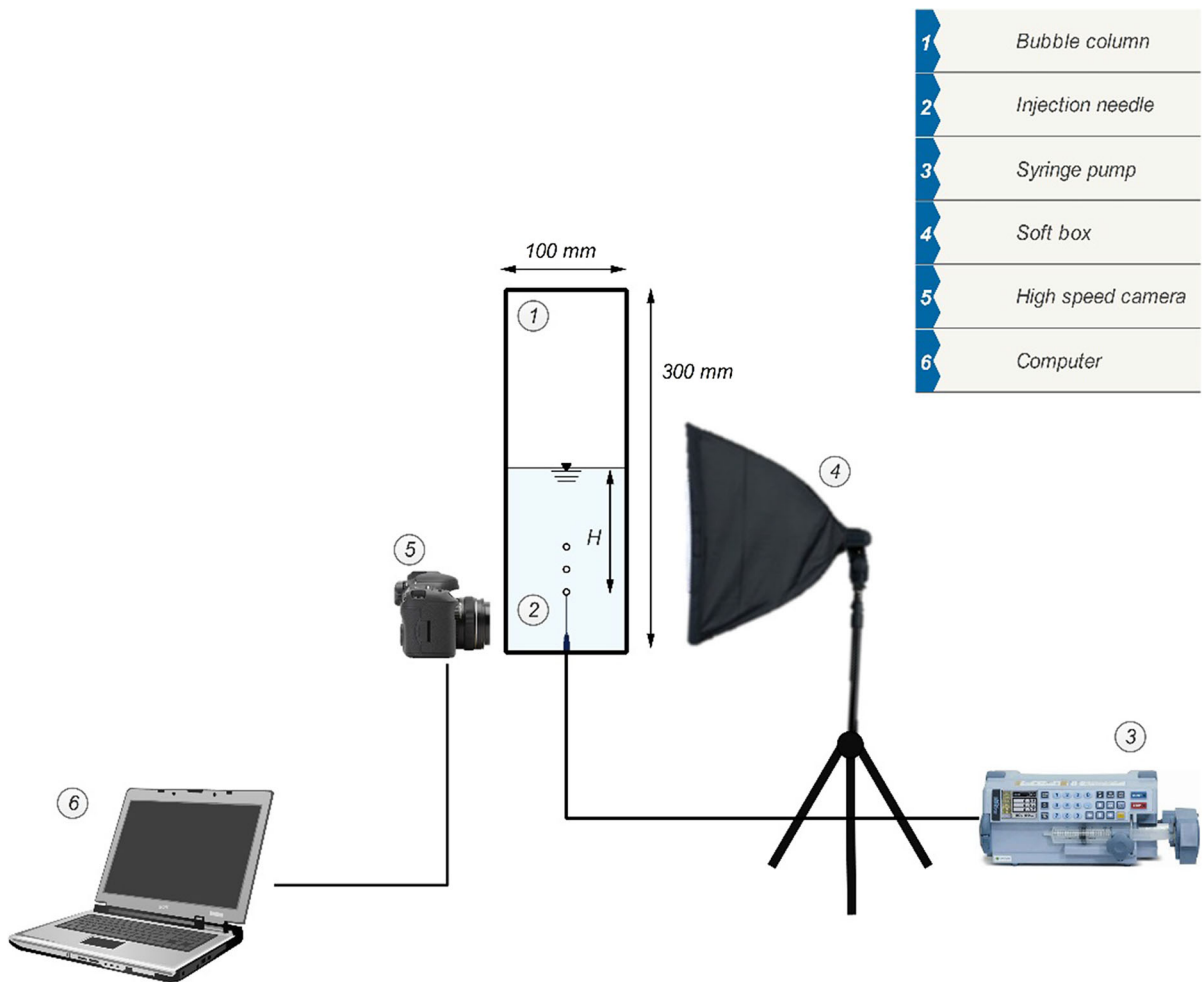
Fig. 3 Schematic view of the experimental apparatus

Table 2 Uncertainties in experimentally measured variables

Parameter	Amount of uncertainty	Uncertainty percentage
Air flow rate	–	3%
Needle diameter	0.005 mm	–
Physical calibration scale	0.005 mm	–
Image calibration scale	1 pixel	–

- Bubble growth happens adiabatically.
- All properties of gas and liquid phases are assumed to be constants and they are measured at room temperature (20 °C).
- Liquid phase in the current project is quiescent, thus the liquid trust force is not considered.
- The pressure of the gas is uniform within the bubble and the influence of gas viscosity is negligible due to high Reynolds number (Re).

- Gas momentum force is negligible compared with other forces acting on the bubble.
- Because the thickness of the orifice is negligible in comparison with equivalent diameters of that, the contact line between needle and bubble is considered to be fixed to the inner rim of the needle.
- The gravity force is neglected because the density of gas phase is much lower than liquid one in this study.
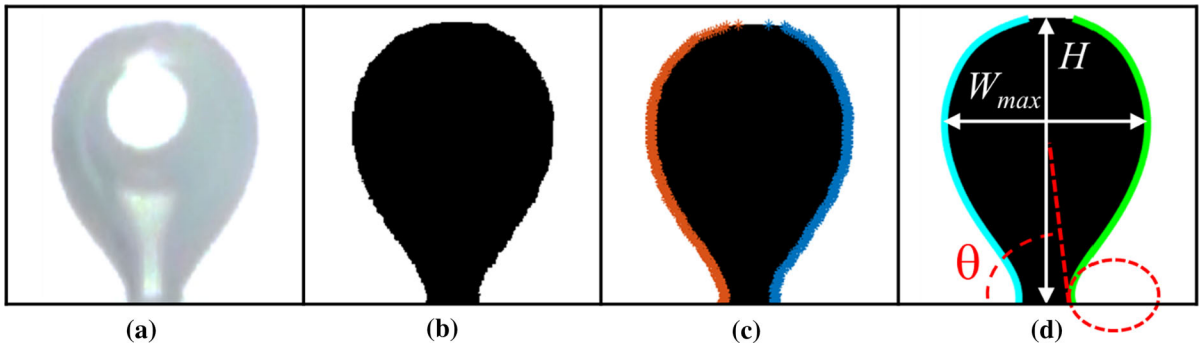
Fig. 4 IP method implementation: **a** original image **b** binary image **c** boundaries gathered and **d** curves fitted to the boundary for square geometry with 1200 mlph flow rate and 5 cm liquid height
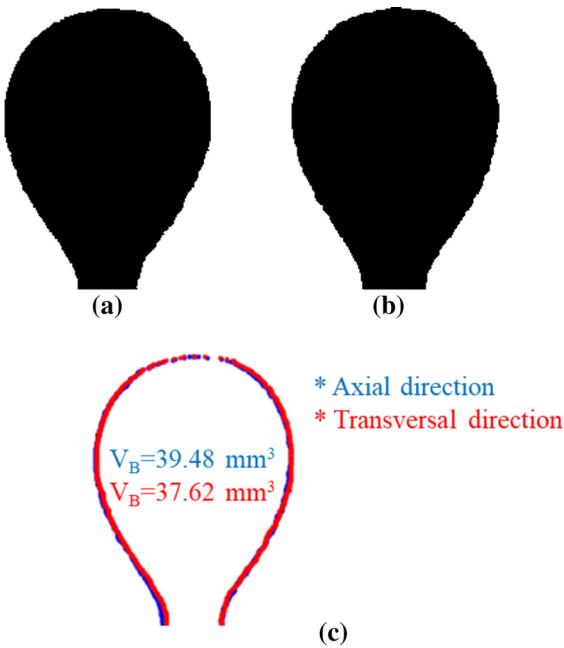

Fig. 5 Bubble near detachment from **a** axial and **b** transversal directions and **c** comparison of boundaries and volumes for triangular orifice, 1000 mlph flow rate, and 5 cm liquid height above the orifice

During bubble formation, when bubbles are very small, the forces holding the bubble to the needle surface (in the negative direction) are larger than the forces that pull the bubbles from the needle (in the positive direction). As the bubble grows, the positive forces grow faster than the negative ones, and the bubble detaches when the positive forces overcome the maximum force that negative ones can exert. The negative forces are surface tension and drag and the positive ones are buoyancy and internal pressure. Forces acting on the bubble and their directions, and characteristics of the bubble are shown in Fig. 7.

A force balance can determine the bubble departure as the following:

$$F_\sigma + F_D + F_B + F_p - m_g a_{CM} = 0, \tag{3}$$

where F, F_D, F_B, F_p, and $m_g a_{cm}$ are surface tension, drag, buoyancy, pressure, and inertia forces, respectively. Since the injection rate and the gas density (in comparison with the liquid density) are small, the gas momentum is negligible compared with other mentioned forces. This is confirmed by the calculation that the gas flow rate is below the critical injection rate predetermined in [4]. The equivalent diameter of the bubble is calculated as the following:
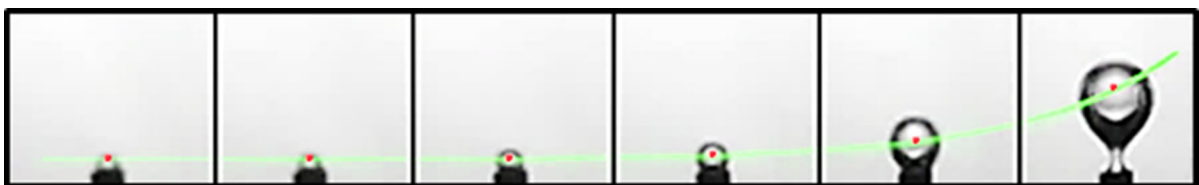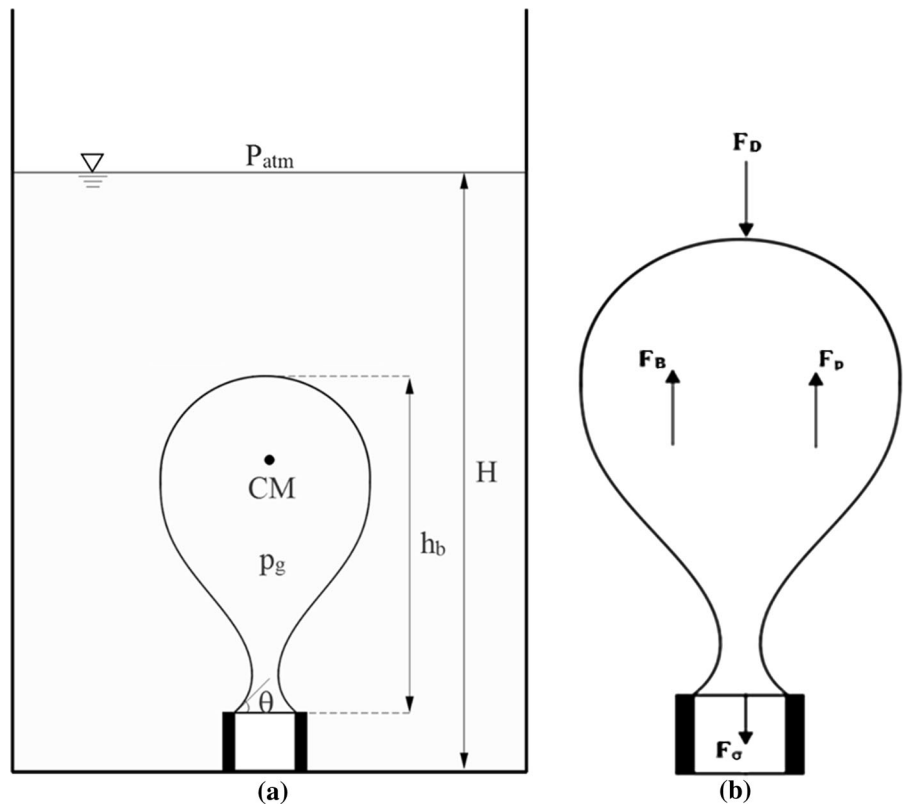

Fig. 6 Bubble's CM displacement for circular geometry with 1200 mlph flow rate and 5 cm liquid height

Fig. 7 **a** Bubble characteristics and **b** schematic of force acting on the bubble

$$V = \pi \frac{D_{eq}^3}{6} \Rightarrow D_{eq} = \left(\frac{6V}{\pi}\right)^{\frac{1}{3}}, \qquad (4)$$

where V and D_{eq} are the bubble volume and the equivalent diameter, respectively. The surface tension force, F, is caused by the attraction of the liquid to the surface that acts around the perimeter of the bubble base. The surface tension force is proportional to the fluid surface tension, σ, and the contact angle, θ:

$$F_\sigma = \sigma P \sin\theta, \qquad (5)$$

where P is the perimeter of the injection needle. When the bubble is growing in a viscous fluid, it will be subjected to drag force. A very rough estimate of this force was made by Keshock and Siegel [25], and this approximation will be used here. In estimating drag force, it is also assumed that the bubble growing away from the needle at a velocity equal to the change of its radius with time, dR/dt. So, the drag force can be calculated as the follows:

$$F_D = \frac{1}{2} \rho_l C_D u_{CM}^2 A_{pro}, \qquad (6)$$

where ρ_l is the density of the liquid, u_{CM} is the CM velocity of a rising bubble, A_{pro} is the projection area of the bubble considering the actual shape, which is equal to $\pi W_{max}^2/4$, and C_D is drag coefficient that can be calculated by Morrison correlation [26] for wide a range of Reynolds number:

$$C_D = \frac{24}{Re} + \frac{2.6\left(\frac{Re}{5.0}\right)}{1 + \left(\frac{Re}{5.0}\right)^{1.52}} + \frac{0.411\left(\frac{Re}{263,000}\right)^{-7.94}}{1 + \left(\frac{Re}{263,000}\right)^{-8.00}}$$
$$+ \left(\frac{Re^{0.80}}{461,000}\right), \qquad (7)$$

where

$$Re = \frac{\rho_l u_{CM} D_{eq}}{\mu_l}, \qquad (8)$$

where μ_l is the viscosity of the liquid phase. For a spherical bubble, which is submerged in a stagnant

fluid, the buoyancy force is equal to the weight of the fluid displaced and is calculated by the following equation:

$$F_B = V(\rho_l - \rho_g)g, \tag{9}$$

where ρ_g and V are the density and the volume of the gas phase, respectively. Finally, the pressure force, which is a result of the contribution of the dynamic excess vapor pressure and capillary pressure, can be written as follows:

$$F_p = (P_g - P_l)A_D, \tag{10}$$

where A_D is the surface area of the needle. P_g and P_l are inside bubble pressure and the liquid pressure values at the tip of the bubble. This term can be expressed by applying Young–Laplace equation:

$$P_g - P_l = \sigma\left(\frac{1}{R_1} + \frac{1}{R_2}\right), \tag{11}$$

where σ is the surface tension between liquid and gas, and R_1 and R_2 are the principal radii of curvature.

For calculating principle radii of the curvature, the bubble surface is divided into many two-dimensional axisymmetric elements as shown in Fig. 8. R_2 is the
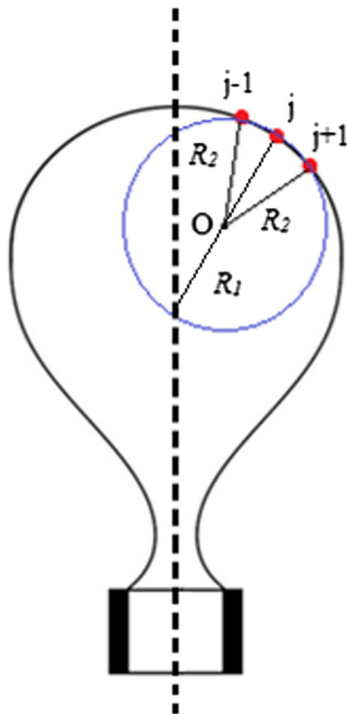

Fig. 8 Schematic of the non-spherical bubble formation model

radius of the circle which passes through the elements $(j-1), j$, and $(j+1)$, and has a center point O; and R_1 is the distance from the bubble axis of symmetry to the element j through the point O. The average of all equivalent radius R_E, which is defined by Eq. (12) is used as the characteristic radius for the term of different pressure:

$$\frac{1}{R_E} = \frac{1}{2}\left(\frac{1}{R_1} + \frac{1}{R_2}\right). \tag{12}$$

So, pressure force can be written as follows:

$$F_p = \frac{2\sigma A_D}{R_E}, \tag{13}$$

The perimeter of needles for the current research are as the following:

$$P = \begin{cases} Circular = 5.03\,\text{mm} \\ Square = 5.76\,\text{mm} \\ Triangular = 6.75\,\text{mm} \end{cases} \tag{14}$$

5 Results and discussions

Circular, square, and triangular cross-sectional geometries are tested for same gas flow rates. Generally, formation of bubbles happens in three stages: weeping, expansion, and detachment. In the first stage, downward forces acting on bubbles dominate and bubbles don't grow. In the second stage, the bubbles are formed slowly. This means upward and downward forces are approximately equal. Then the process of detaching starts by forming a neck near the bubble base. In this stage, the influence of buoyancy is increased as the curving inward of the neck increases the volume being acted upon by buoyancy. This causes the upper region to accelerate upward. In other words, upward forces grow faster than downward ones in this stage and as a result the bubble's velocity and acceleration increase up to the detachment of the bubble.

Figure 9 shows a sequence of bubble formation for 800 mlph flow rate and 5 cm liquid height above the needle for three geometries. As shown in this figure, it is clear that the geometry of injection affects the bubble characteristics. It is observed that the smallest bubbles with lowest heights are related to circular geometry.
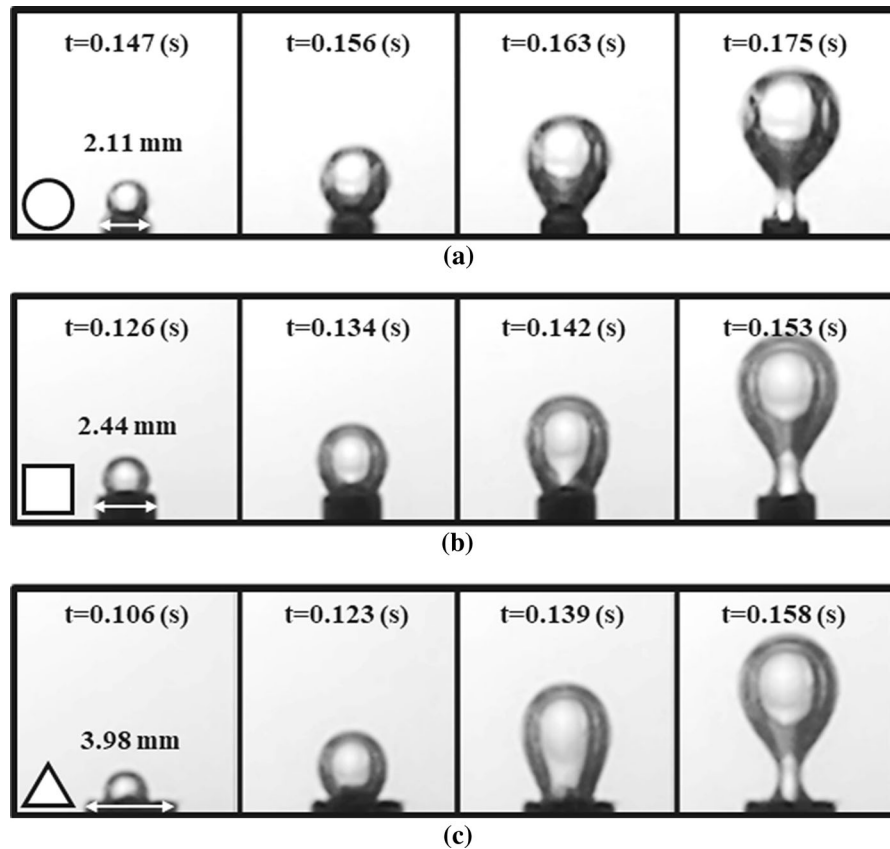
Fig. 9 Sequence of bubble formation with the gas injection rate of 800 mlph and 5 cm liquid height for **a** circular **b** square and **c** triangular needle geometries

In order to calculate the volume, height and contact angle of bubbles during the formation process, boundary points of bubbles are captured with the IP method. Afterwards, a polynomial equation is fitted to the boundary. For the sequence happening in Fig. 9, resulted boundaries from IP are shown in Fig. 10.

In order to evaluate the dynamics of bubble formation process for different geometries, a normalized time, t^*, is defined as follows:

$$t^* = t/t_f, \tag{15}$$

where t and t_f are the elapsed time and total time of bubble formation, respectively. In order to capture the bubble formation dynamics and understand the effect of injection geometry, the CM displacement is measured based on Eq. (2). As an example, the positions and normalized positions of bubble's CM versus the normalized time (t^*), for 1000 mlph flow rate, 5 cm liquid height, and different geometries are shown in Fig. 11.

As seen in Fig. 11, bubbles generated from the triangular needle have the highest CM position. This shows that these bubbles may have the maximum height or the thinnest bottom in comparison with the others. Also, bubbles which rise from the square needle have the lowest CM position which means these bubbles may have lower height or the broadest bottom in comparison with the others (4.540, 4.367, and 4.777 mm for circular, square, and triangular orifices at detachment respectively). Moreover, according to different stages of bubble formation, it is clear that the expansion stage lasts longer than the other stages. Also, from the normalized figure, it can be concluded that shape of the orifice has an effect on bubble characteristics.

By having the position of bubble's CM, its velocity can be easily obtained via:

$$v_i = (x_i - x_{i-1})/\Delta t, \tag{16}$$

Fig. 10 Curves are fitted to the boundaries of bubbles generated with **a** circular **b** square and **c** triangular cross-sectional geometries for the sequence of Fig. 9
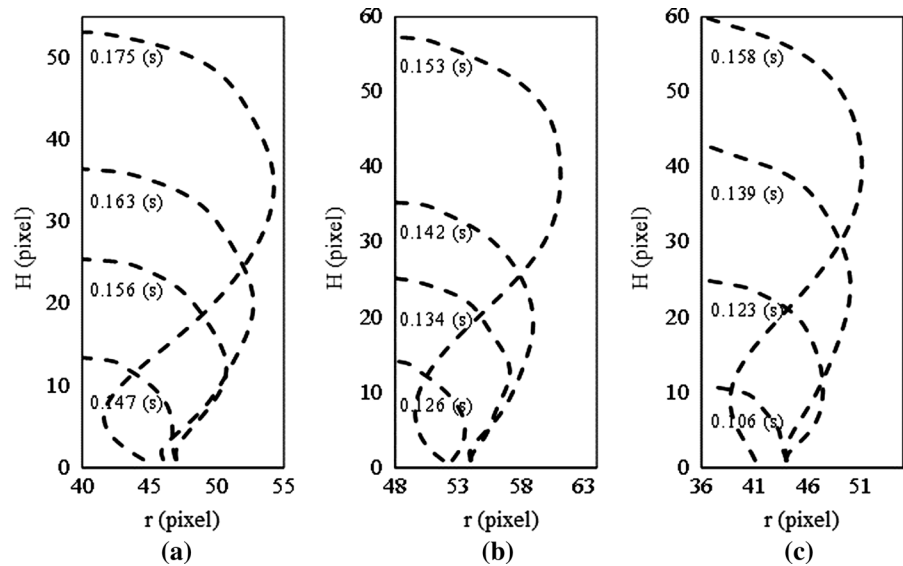
where v_i is the velocity of CM at the ith time step, x_i and x_{i-1} are the positions of CM at ith and $(i-1)$th time steps, respectively, and Δt is the time step based on photography precision and it is equal to 1/1200 s. So, the diagram of velocity and normalized velocity of CM versus time for 1000 mlph and 5 cm liquid height is obtained and shown in Fig. 12.

As seen in Fig. 12, bubbles generated from the circular and square needles have the largest and smallest CM velocity at detachment, respectively (204.188, 176.158, and 178.954 mm/s for circular, square, and triangular orifices at detachment respectively). By comparing the results of Figs. 11 and 12, it could be understood that although the bubbles formed from the circular needle have higher CM velocity, they have a lower CM position at the detachment. As shown in Fig. 11, CM of bubbles generated from the circular orifice is lower than those of the triangular one but these values become closer as time reaches the detachment.

The surface tension force is much different from the other forces, since the shape of the contact line, which is the major difference between different orifices, affects this force directly. However, it should be noted that different shapes must be compared based on their perimeter and contact angle. According to data presented in (14), the triangular orifice has the largest perimeter and it seems that it should have the most surface tension force and largest contribution of downward forces, and therefore the velocity of its

CM should be lower rather than others; but Fig. 12 shows that this justification isn't necessarily correct without considering the effect of contact angle. On the other hand, changing a force in the balance of forces results in changes in the other forces and the other characteristics of the bubble. Therefore, all forces acting on a bubble are coupled with each other during the formation and simultaneous investigations are crucial. Also, from the normalized figure, it can be seen that shape of the orifice has a significant influence on bubble CM velocity.

Similar to the velocity, the acceleration can be found by:

$$a_i = (v_i - v_{i-1})/\Delta t, \qquad (17)$$

where a_i is the CM acceleration at ith time step, and v_i and v_{i-1} are the velocities of CM at ith and $(i-1)$th time steps, respectively. The diagram of acceleration and normalized acceleration of CM versus time for 1000 mlph and 5 cm liquid height is obtained and demonstrated in Fig. 13.

According to Fig. 13, bubbles generated from the circular and square needles have the highest and lowest CM accelerations, respectively. As illustrated in this figure, weeping stage has approximately zero acceleration, and this value is affected significantly in detachment by the dimension of the bubble. The trends of Fig. 13 are similar to those in Fig. 12 and same justifications can be used.
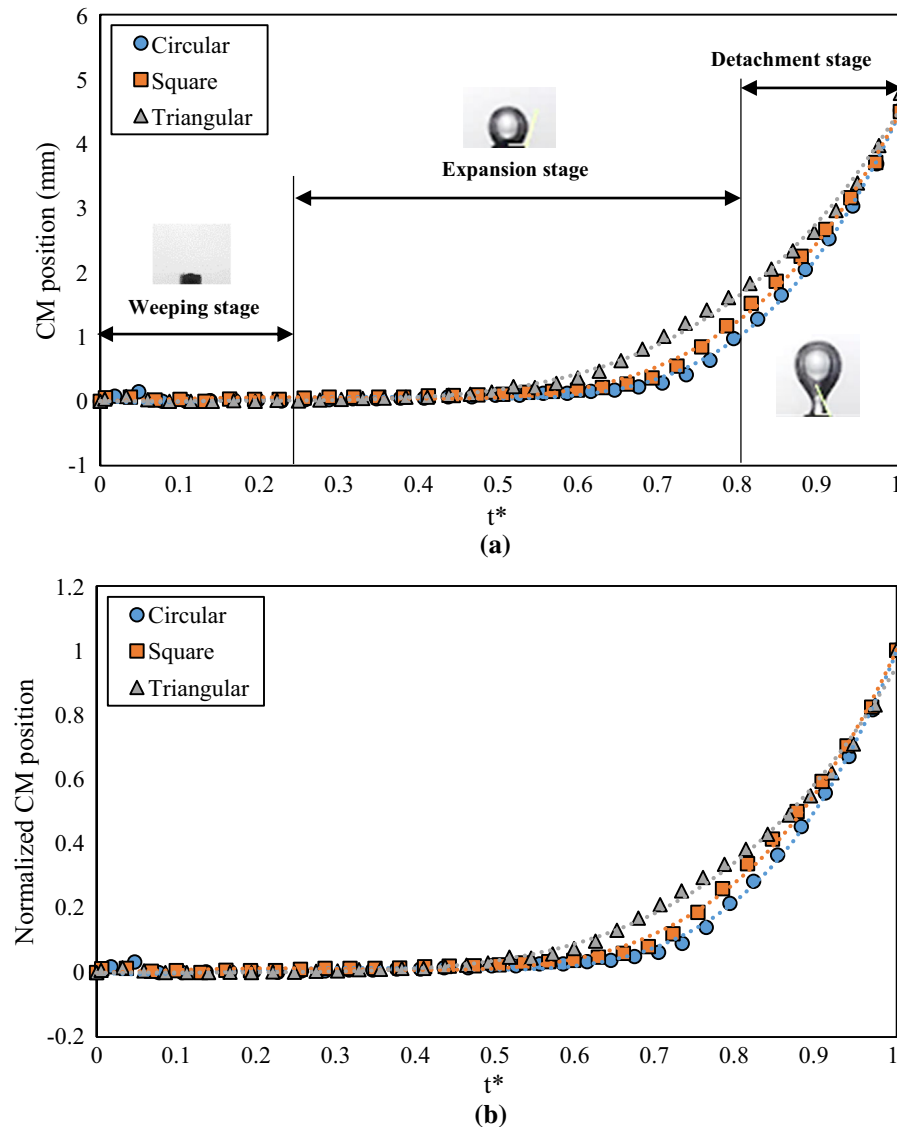
Fig. 11 **a** CM position and **b** normalized CM position with respect to the detachment value versus t^* for 1000 mlph flow rate and 5 cm height of the liquid

In order to investigate the influence of liquid height, tests were performed with three liquid heights of 5, 10, and 15 cm, and effects of these heights on three major parameters of bubbles including frequency, volume, and height of bubbles at detachment time are investigated, which are illustrated in Fig. 14. It can be seen in Fig. 14a that by increasing height of the liquid column, the frequency of formation decreases. This is because by increasing liquid height the pressure of the liquid on the bubble increases and it delays the detachment. In contrast, increasing bubble volume

with increasing height (Fig. 14b) can be easily justified with this reality that volume of the bubble at detachment has a reverse relation with the frequency of formation at constant air injection rate. Finally, bubble height has a reverse relation with a height of liquid column (Fig. 14c). It can be justified by this fact that with increasing column height, the pressure of the liquid acting on the bubble tip increases and as a result bubble has to do its growth in the transverse direction which resulted lower in height and more obese bubbles. So it can be said that liquid height has a
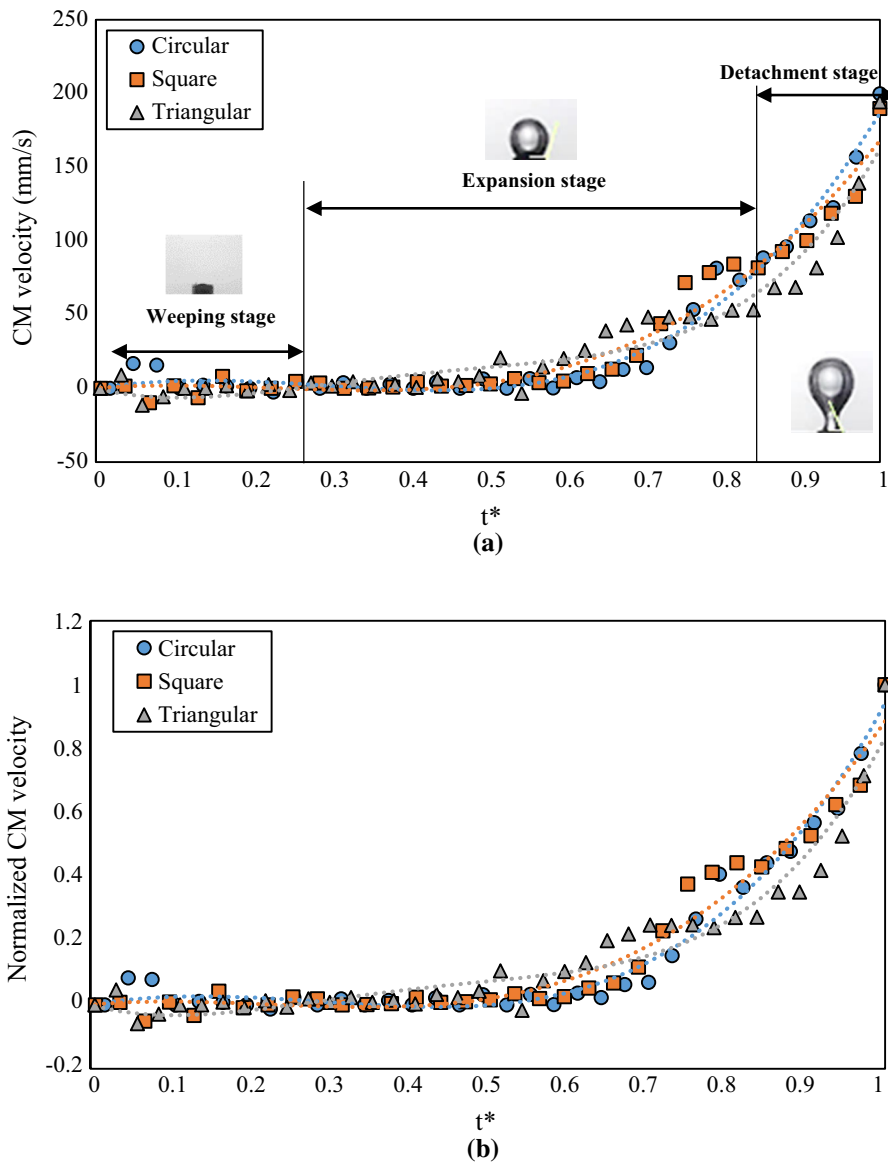
Fig. 12 **a** CM velocity and **b** normalized CM velocity with respect to the detachment value versus t^* for 1000 mlph flow rate and 5 cm height of the liquid

noticeable effect on bubble characteristics, considering that liquid height wasn't changed too much (just 10 cm). For instance, for square geometry and 600 mlph flow rate, frequency, volume, and height of the bubbles changed 6.75, 6.90, and 11.87% with 10 cm liquid height change respectively. This is in contrast with some previous researches [12] which mentioned that liquid height does not have a noteworthy effect on the mechanism of bubble formation.

The effective forces acting on a bubble are functions of equivalent diameter, velocity, contact angle, Re, and C_D at the detachment. The effect of gas flow rate on these parameters for different geometries and 15 cm liquid height above the needle is shown in Fig. 15. As illustrated, diameter, velocity, and Re increase with increasing the gas flow rate, while C_D and contact angle decrease with increasing the gas flow rate. Moreover, at a constant flow rate, the square and circular needles have the most and least equivalent

Fig. 13 a CM acceleration and **b** normalized CM acceleration with respect to the detachment value versus t^* for 1000 mlph flow rate and 5 cm height of the liquid
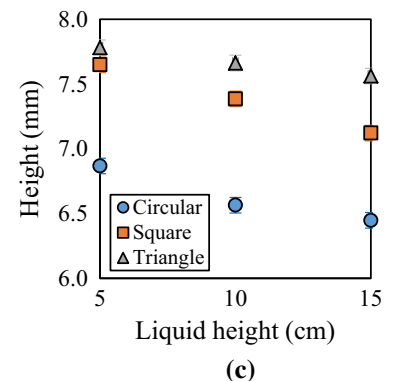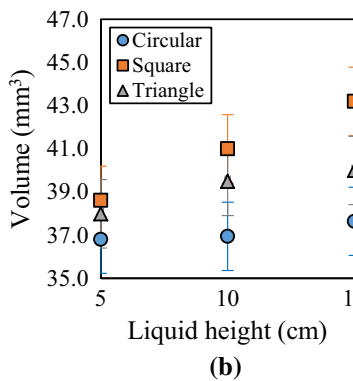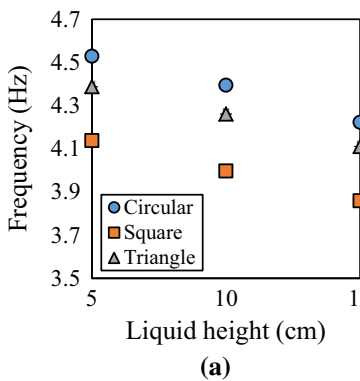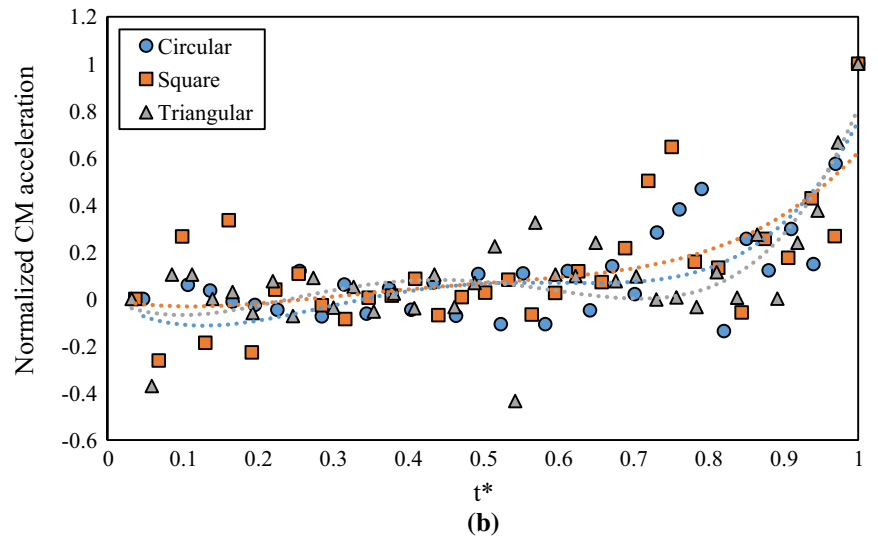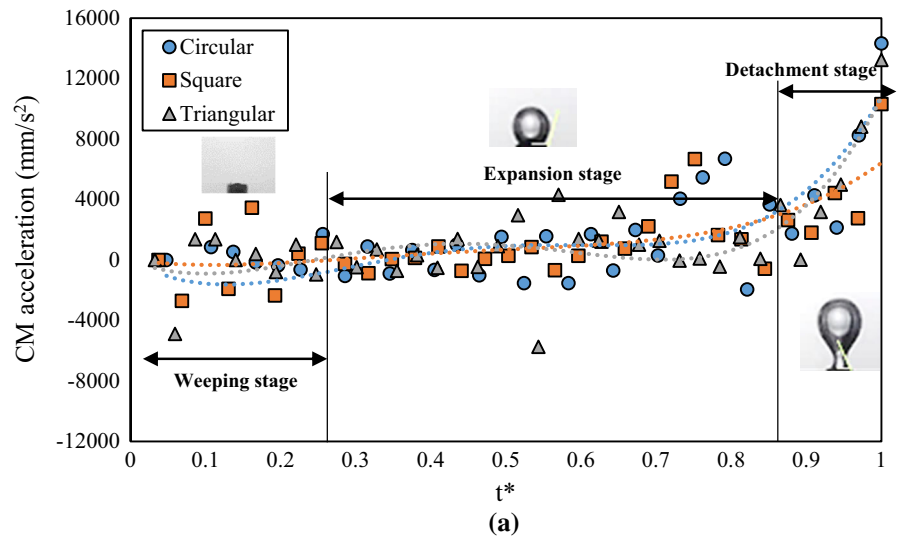

Fig. 14 a Frequency **b** volume at detachment and **c** height at the detachment of the bubble versus liquid height for 600 mlph flow rate
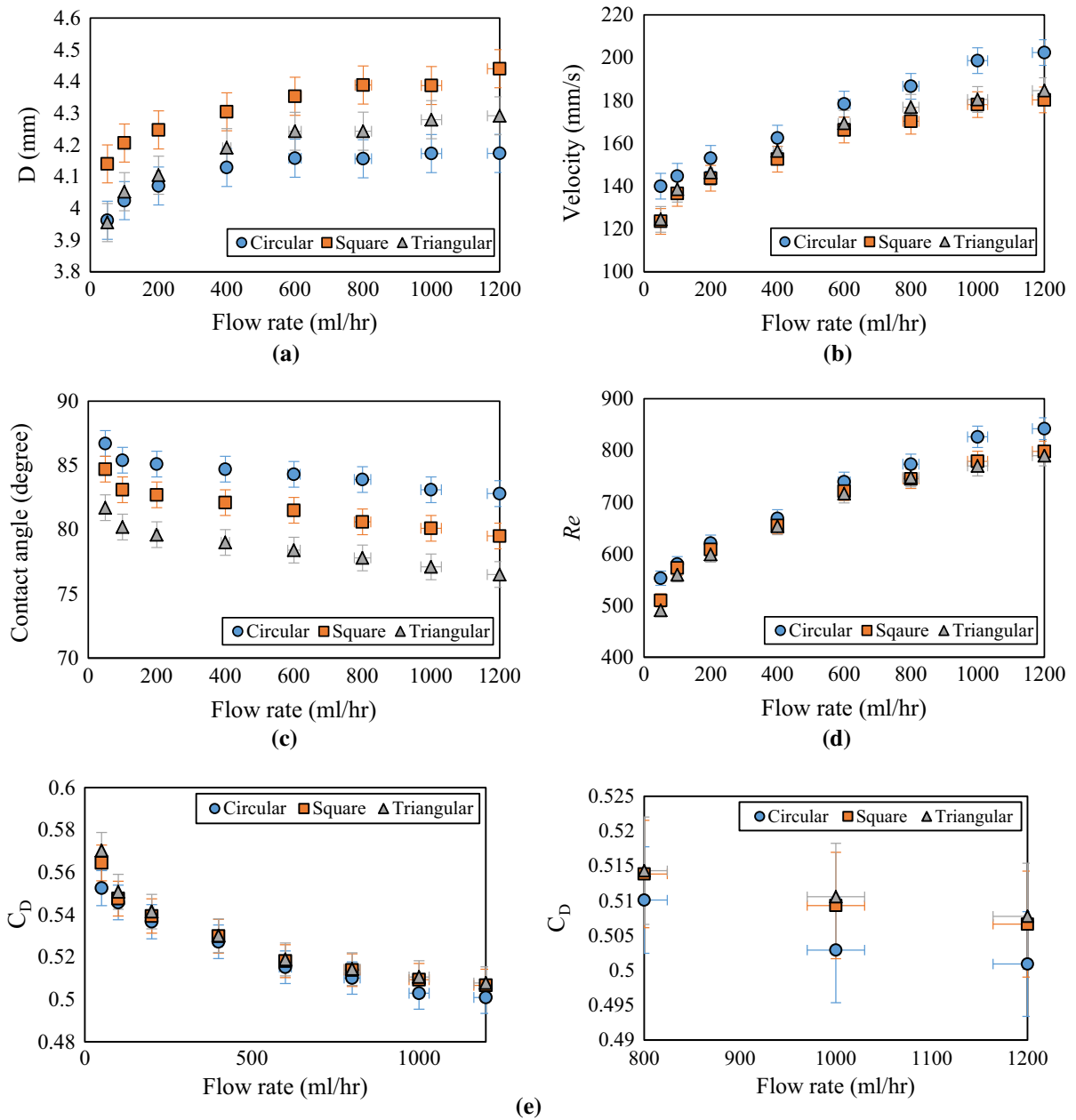
Fig. 15 **a** Diameter of bubbles **b** velocity of bubbles **c** contact angle **d** *Re* and **e** drag coefficient at detachment time versus gas flow rate and magnified chart of drag coefficient for circular, square, and triangular geometries with 15 cm liquid height above the needle

diameters as shown in Fig. 15a. This shows surface tension force has more contribution at detachment for square orifice rather than the circular one (this matches with Fig. 17). That the contribution of surface tension force is larger implies that the other forces need to grow larger to overcome it. So, the major important upward force, buoyancy, needs to be larger and

consequently larger detachment volume. Larger detachment volume is consequent of more gas injection into the bubble and because the orifices have the same cross-sectional area, it means that more time of injection needs to achieve to a higher volume. According to Fig. 15b, rising bubbles from the circular needle have the highest velocities at detachment while

bubbles generated with the square needle have the least velocities. This corresponds to Fig. 12 and the justification presented there.

The other important parameter is the contact angle and its change versus the gas flow rate is illustrated in Fig. 15c. For each value of gas flow rate, the contact angle decreases from the circular to the square and then to the triangular needle. The circular geometry has the lowest perimeter and the largest contact angle. Figure 17 shows the effect of perimeter dominates the effect of contact angle and results in the lower contribution of surface tension force for this geometry with respect to the other ones, so the volume of the bubbles generated from the circular needle is the smallest. In contrast, in triangular geometry, the effect of perimeter dominates the effect of contact angle and this results in the higher contribution of surface tension force with respect to the circular needle. It should be noted that the small contact angle at detachment (lower than 90°) corresponds to high wettability of the solid surface material.

It is clear that by increasing the equivalent diameter and velocity magnitude, Re must be increased. The circular needle, as mentioned before, has the lowest and highest equivalent diameter and velocity, respectively, but the effect of velocity dominates and results in higher Re (Fig. 15d). Similar justification can be utilized for the square and triangular geometries; this means the effect of higher bubble diameter for the square needle dominates the effect of lower velocity in comparison with the triangular needle and as a result, the bubbles generated with the square needle have higher Re. Figure 15e shows the variation of C_D with respect to the gas flow rate. Reynolds number is a significant parameter affecting the drag coefficient. As shown in this figure, C_D has a reverse relation with Re and rising bubbles from triangular and circular needles have the most and least drag coefficients, respectively. But as can be seen in the magnified chart, drag coefficient has a very low dependence on the shape of the orifice. Besides, with a rough estimation, as the drag coefficient gets larger when the shape changes from the streamlined body to spherical, bubbles generated from circular geometry have more spherical shape than triangular ones at least at detachment point, although this difference is small.
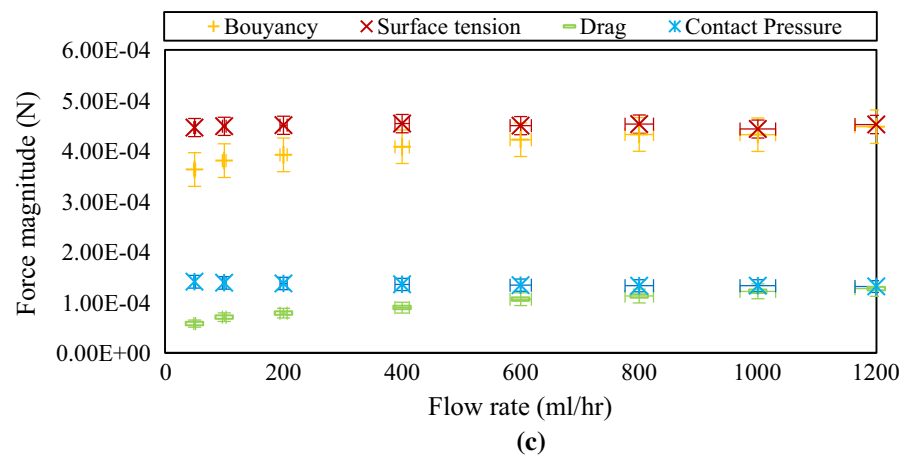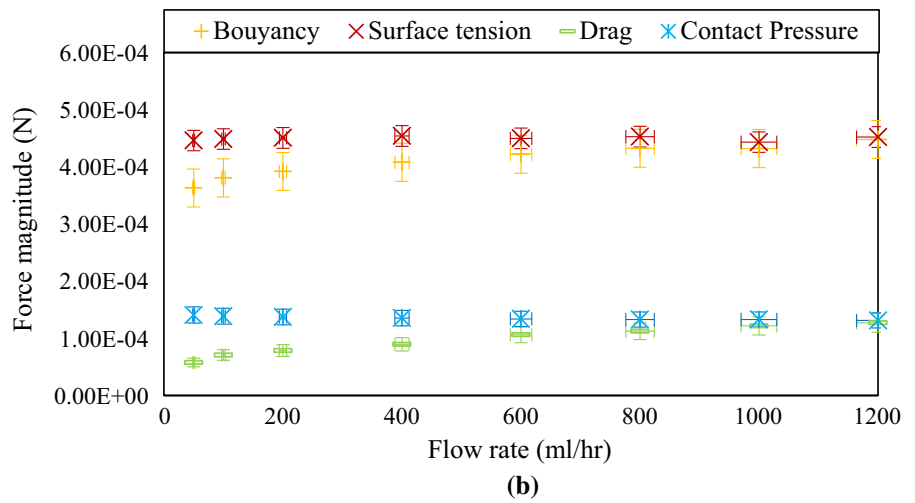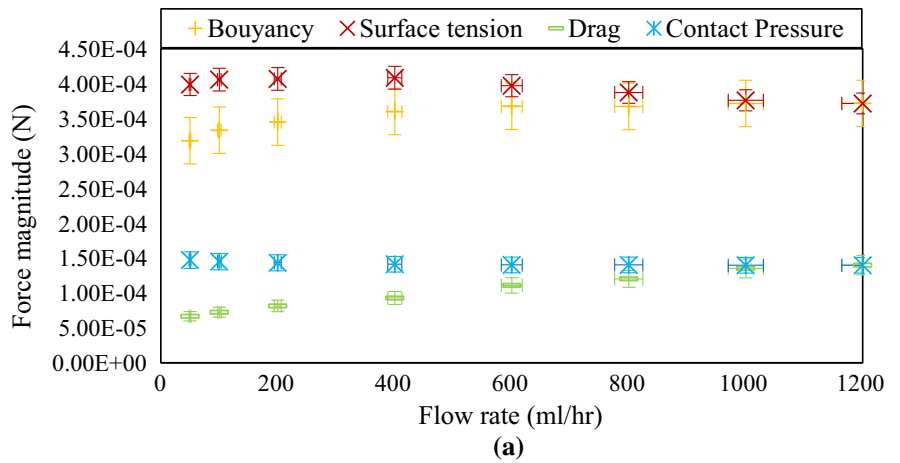
The vertical forces acting on bubbles are computed by using Eqs. (5) to (13), and their values are plotted as a function of the gas flow rate in Fig. 16. Relative uncertainty bars are also shown. Moreover, the contribution of each force at different flow rates are computed and illustrated in Fig. 17. As shown in these figures, as long as the equivalent diameter of the bubble increases with flow rate, the buoyancy force increases as well and this force dominates. However, as the contact angle decreases by increasing the gas flow rate, the magnitude of surface tension force decreases, and as a result, the contribution of surface tension force decreases too. Also, by considering Eq. (13), contact pressure force and its contribution decreases with increasing gas flow rate, since this force has reverse relation with the equivalent diameter which increases with increasing gas flow rate. Finally, drag coefficient and its contribution increase with increasing gas flow rate. Drag coefficient based on Fig. 15e decreases with increasing gas flow rate while the equivalent diameter and velocity magnitude of detachment increase, so that increasing them overcome decreasing drag coefficient and results in larger magnitude and contribution of drag coefficient.

Also, as shown in Fig. 17, the contribution of surface tension force for bubbles generated from triangular and square needles are larger than the ones generated from circular needle. Although based on Fig. 19, contact angle of bubbles generated from circular needles are bigger than others, the lower perimeter of circular needle dominates contact angle and resulted in a lower contribution of the surface tension force. This phenomenon resulted in more power of downward forces in the square needle, which resulted in more formation time and more injected gas and as a result larger volume at detachment time. On the other hand, bubbles generated from square needle have a larger contribution of buoyancy force due to the larger volume. Unlike this, since the contact pressure force has reverse relation to the bubble diameter, the lower contribution is given to this force in the square orifice. Finally, drag force in circular needle has a larger contribution in comparison with other needles. It can be said that although bubbles generated from circular needle have a smaller diameter, the bigger velocity at detachment overcomes diameter and as a result drag force has a larger contribution in this needle.

A sequence of bubble growth from the circular orifice with the highest air injection rate and 5 cm liquid height above the orifice is illustrated in Fig. 18. During the weeping stage, (t* < 0.25), the bubble is

Fig. 16 Variation of vertical forces acting on bubbles generated with a circular b square and c triangular cross-sectional needles with 15 cm liquid height above the needle at detachment time

Fig. 17 Contribution of vertical forces acting on bubbles generated with **a** circular **b** square and **c** triangular cross-sectional needles with 15 cm liquid height above the needle at detachment time
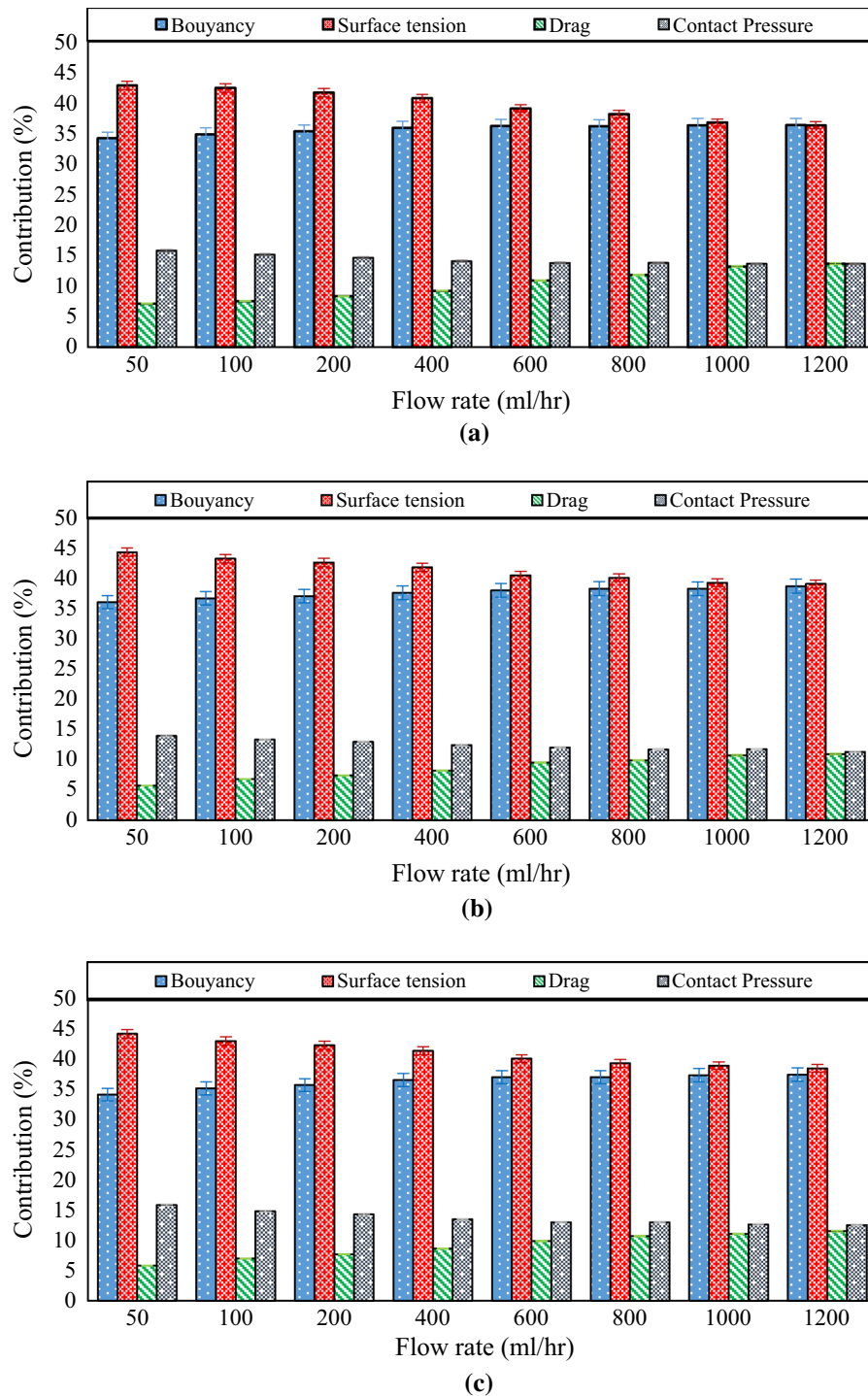
Fig. 18 Bubble formation process with the contact angle for the circular needle with 1200 mlph flow rate and 5 cm liquid height above the needle

growing from the orifice and its shape is a portion of a sphere. As the volume of the bubble increases, the buoyancy effect increases (Fig. 16). As the bubble becomes large enough, it becomes elongated due to the forces tend to lift the upper part of the bubble. The lower part of the bubble is still attached to the orifice tip. During this expansion stage ($0.25 < t^* < 0.85$) the rate of change of the CM is almost constant with time as shown in Fig. 11. For $t^* > 0.85$, the bubble is in the detachment process by forming a neck near the orifice tip. In this stage, the produced neck increases the volume of the bubble as well as the buoyancy force. This causes acceleration on the upper part of the bubble as described in Figs. 11, 12 and 13. The acceleration is caused by what is essentially a positive feedback effect. Whereby the collapsing of the neck is responsible for increasing the rate of the necking process which is due to increasing the contribution of the buoyancy force. This finally leads to bubble detachment and breaking the neck.

Figure 18 depicts a sample sequence of evolution procedure of the contact angle. Three stages of bubble growth can be identified by different behaviors of the contact angle. As the bubble appears at the tip of the orifice, the contact angle increases rapidly and changes from an acute angle to an obtuse one. The partial buoyancy force increases until the contact angle reaches its maximum around 120° which is more or less maintained constant during the bubble elongation phase due to the flow rate and the shape of the orifice. This contact angle lasts until the partial buoyancy force acting on the upper region of the bubble become large enough to pull the bubble upward and form a neck. After formation of the neck, the contact angle decreases and once again becomes acute as it begins to pinch off indicating bubble detachment. This procedure is illustrated in Fig. 19 for 5 cm liquid height above the needle and 50 mlph flow rate of injection for three geometries. As shown in this figure circular geometry has the most contact angle at any time. Also,

bubbles generated from square needles have the least contact angle.

Using Eqs. (3)–(13), it is possible to approximate the vertical forces acting on the bubble as it grows. In Fig. 20 these forces are plotted as a function of time. The results are qualitatively similar to the force evolution trends of Duhar and Colin [27]. The upward buoyancy force, F_B, is equal to zero for $t^* < 0.25$ (weeping stage) because there is no contact with liquid below the bubble until the contact angle rises above 90° and the bubble resembles a truncated sphere. From this point, the volume of the bubbles increases dramatically and this is resulted increasing of buoyancy force during the expansion and detachment stages. The upward pressure force, F_P, due to its dependency on the differential pressure (Eq. (10)), is maximum near the beginning of the bubble growth when it is hemispherical and the pressure difference is maximum. Subsequent to this point in time this force monotonically decreases, generally following the trend of the gas pressure evolution, which was discussed by Bari and Robinson [18]. The surface tension force, F, is downwardly directed and acts to keep the bubble fixed to the wall. It has an absolute maximum value when the bubble is hemispherical in shape as the sine function in Eq. (5) is unity. Changing procedure of F_C magnitude is similar to the trend of changing contact angle, which was shown in Fig. 19. Since the magnitude of the surface tension force is large in any stage of formation of bubble in comparison with other forces, it can be concluded that geometry of the needle that directly affects contact angle, play a significant role, not only at detachment moment and on maximum volume of the bubble, but also during the bubble evolution. The downward drag force, F_D, due to Eq. (6), is proportional to the bubble volume and the square of the velocity magnitude. So, by increasing of velocity magnitude (Fig. 12) and bubble volume (Fig. 15a) during formation of the bubble, it can be easily concluded that magnitude of
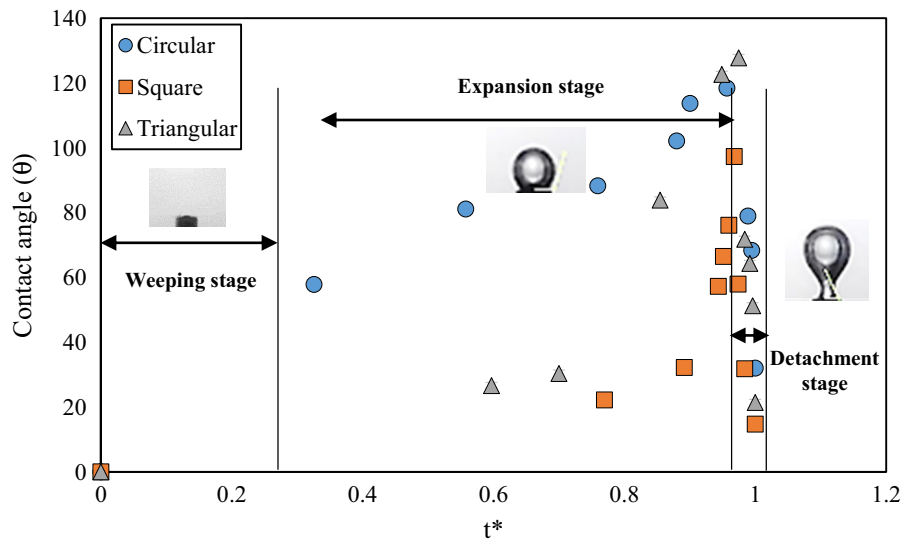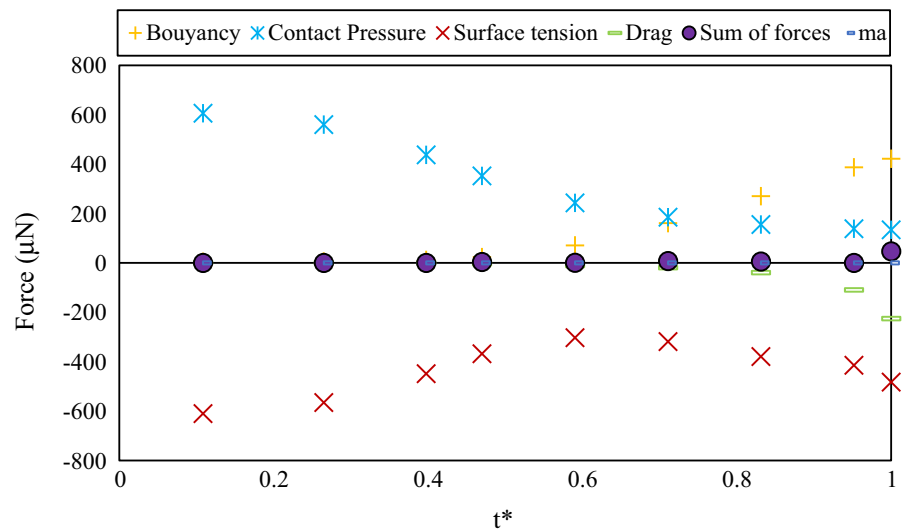
Fig. 19 Contact angle at detachment versus t* for 5 cm liquid height and 50 mlph flow rate

Fig. 20 Vertical forces acting on the bubble during its formation for the circular needle at 600 mlph and 5 cm liquid height above the needle


this force increases whatever time gets closer to the departure moment and its growth becomes faster at detachment stage. As seen in Fig. 20, the contribution of inertia force (*ma*) is small in comparison with other forces and can be neglected especially at expansion stage. This matter could be justified by this reality that although the magnitude of acceleration is considerable particularly at detachment stage, amount of mass of the bubble is low enough for neglecting the production of them. On the other hand, the balance of forces that is taken to characterize the detachment of the bubble should be satisfied during the whole bubble evolution.

For this purpose, as illustrated in Fig. 20, summations of vertical forces acting on the bubble during its formation were computed, which are near zero. This is verifying the assumptions considered for computing forces.

Another major parameter of the bubble is the frequency of formation which is shown in Fig. 21. As shown in this figure frequency of formation increases by increasing gas flow rate and has approximately linear relation with it in the range of operating conditions of current work. Also, the circular needle has the most frequency, then triangular and square

Fig. 21 Frequency of formation versus gas flow rate for 15 cm liquid height
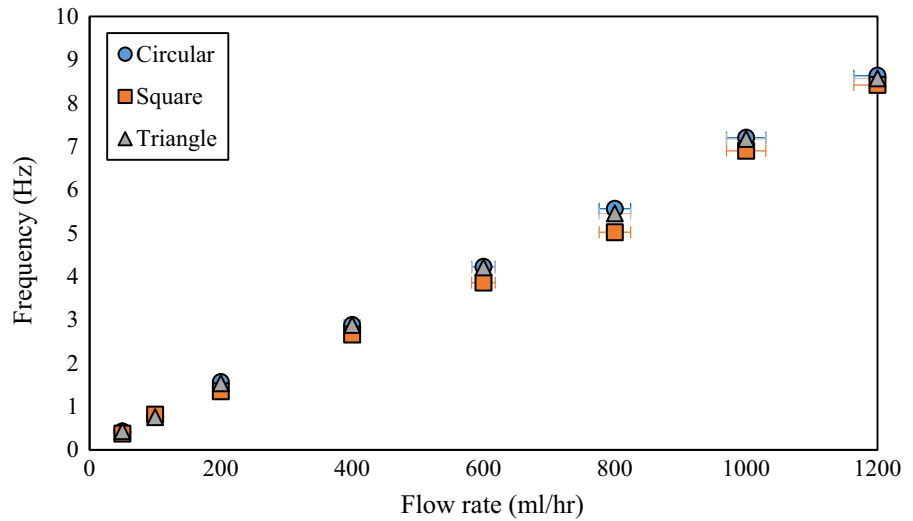
ones. Above conclusion can be easily justified by this reality that the frequency of formation has reverse relation to the bubble volume at constant air injection. Based on Fig. 15a, square and circular needles have the most and the least bubble diameters respectively. So, bubbles that are generated from circular and square geometries have the most and the least frequency of formation respectively. Furthermore, by increasing gas flow rate, equivalent diameter and as a result volume increases too, but the increasing gas flow rate dominates volume and resulted in a larger frequency of formation.

In order to investigate the shape of the bubble, height of the bubble at detachment is defined as the

distance between the needle tip and the top of the bubble. Figure 22 demonstrates the height of bubble versus gas flow rate for 15 cm height of the liquid above the needle and for three geometries. As shown in this figure bubbles generated from triangular and circular geometries have the most and the least height respectively at any gas flow rates. Also, the height of the bubble at detachment is almost independent of gas flow rate while shows a bit increase with increasing gas flow rate. For instance, in the triangular orifice, by increasing gas flow rate from 50 to 1200 mlph, the bubble height shows about 3.5% increase (from 7.385 to 7.649 mm). Since the bubble volume increases with increasing gas flow rate, it can be concluded that

Fig. 22 Height of bubbles at detachment versus gas flow rate for 15 cm liquid height
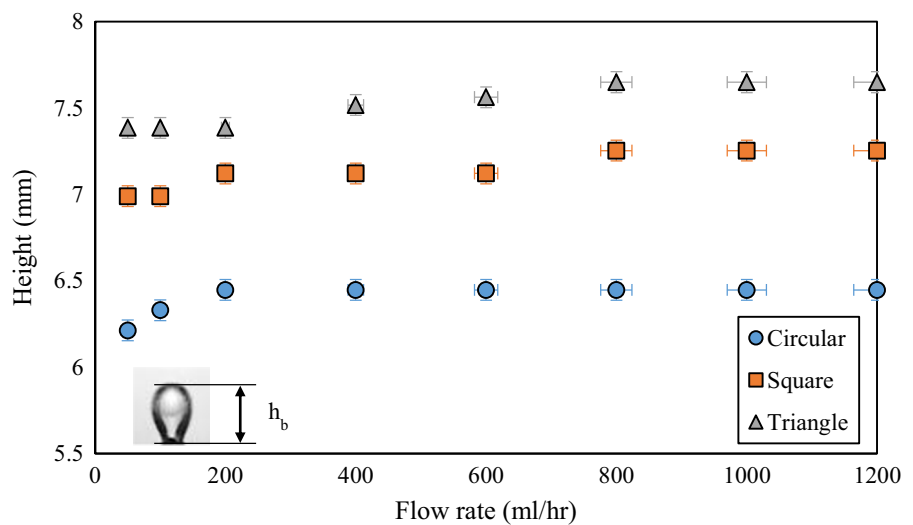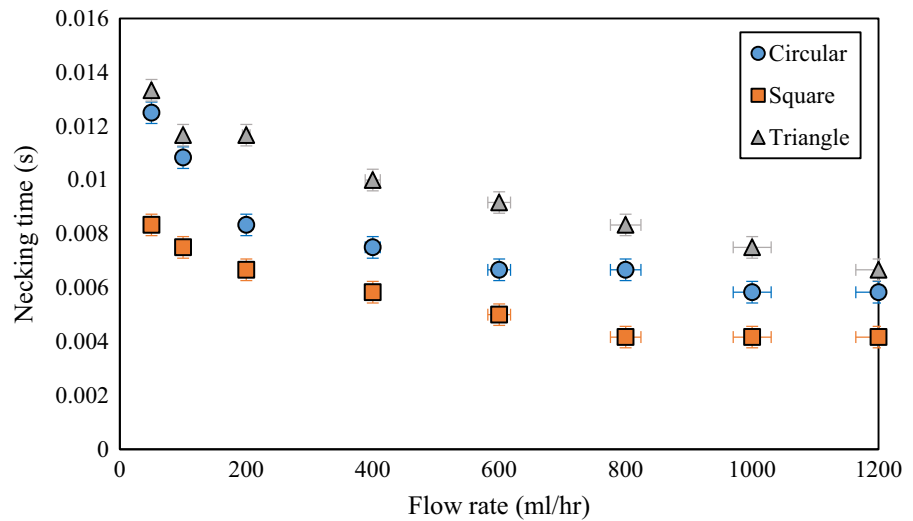
Fig. 23 Necking time versus gas flow rate for 5 cm liquid height and the three geometries

enlargement of bubble almost happens in the transverse direction. On the other hand, it can be concluded that the height of the bubble at detachment has a direct relation with perimeter of the orifice, i.e. orifice with higher perimeter generates bubble with higher height at detachment moment.

Figure 23 demonstrates necking time versus the gas flow rate for 5 cm liquid height for three geometries. Necking time is defined as the time interval between the start of necking and bubble detachment (time of detachment stage). As shown in this figure, the square and triangular geometries have the most and least necking times, respectively. It means that time between necking and detachment at a specific flow rate in the square needle is the lowest, and weeping and expansion stages last longer. Moreover, necking time has a reverse relation with gas flow rate, because with increasing gas flow rate a larger contribution of the bubble is affected by buoyancy as shown in Fig. 17. The larger magnitude of buoyancy force, the easier detachment of the bubble and lower necking time.

6 Conclusion

Effects of cross-sectional geometry of air injecting needle, the height of water above it and the gas flow rate through it on the mechanism of bubble formation are investigated experimentally. Bubbles' contact angle and their equivalent diameter, frequency, height,

and necking time are measured. The effective forces magnitude and their contribution have been investigated at detachment and formation time. The brief results are as the following:

- The shape of the orifice has a significant influence on characteristics of the bubble during its evolution.
- The most and least amounts of bubbles' CM velocity and acceleration at detachment happens for circular and square shapes of orifices with the same cross-sectional area, respectively.
- In a same cross-sectional area of the orifice, contribution of surface tension and buoyancy forces are the smallest for the circular shape, while the contribution of the drag force is the largest. Moreover, the lowest contribution of contact pressure force happens for the square shape.
- Bubbles generated from circular and square needles have the most and least contact angles at any time of formation.
- In a same cross-sectional area, the bubbles generated from the square and triangular shapes orifice are larger than ones formed from circular one.
- Balancing the effective forces during the formation of bubbles demonstrates surface tension force has the largest contribution among the forces acting on the bubble during its evolution.
- The shape of the injecting needle affects both the contact angle and the bubble characteristics, not only at detachment time but also in all stages of formation.

- The height of the bubbles at detachment time is almost independent of the gas flow rate and has a reverse relation with the equivalent diameter of the orifice.
- Necking time changes significantly with the shape of the orifice. Triangular and square orifices have the largest and the least necking time respectively.

References

1. Davidson JF, Schüler BOG (1960) Bubble formation at an orifice in a viscous liquid. Chem Eng Res Des 75:S105–S115

2. Satyanarayan A, Kumar R, Kuloor NR (1969) Studies in bubble formation—II bubble formation under constant pressure conditions. Chem Eng Sci 24(4):749–761

3. Sada E, Yasunzshz A, Katoh S, Nishioka M (1978) Bubble formation in flowing liquid. Can J Chem Eng 56:669–672

4. Oguz H, Prosperetti A (1993) Dynamics of bubble growth and detachment from a needle. J Fluid Mech 257(1):111–145

5. Takagi S, Prosperetti A, Matsumoto Y (1994) Drag coefficient of a gas bubble in an axisymmetric shear flow. Phys Fluids 6(9):3186–3188

6. Vafaei S, Angeli P, Wen D (2011) Bubble growth rate from stainless steel substrate and needle nozzles. Colloids Surf A Physicochem Eng Asp 384(1–3):240–247

7. Ramakrishnan S, Kumar R, Kuloor NR (1969) Studies in bubble formation—1 bubble formation under constant flow conditions. Chem Eng Sci 24:731–747

8. Ramakrishnan S, Kumar R, Kuloor NR (1969) Studies in bubble formation—I bubble formation under constant flow conditions. Chem Eng Sci 24(4):731–747

9. Gaddis ES, Vogelpohl A (1986) Bubble formation in quiescent liquids under constant flow conditions. Chem Eng Sci 41(1):97–105

10. Terasaka K, Tsuge H (1993) Bubble formation under constant-flow conditions. Chem Eng Sci 48(19):3417–3422

11. Hao Y, Prosperetti A (1999) The effect of viscosity on the spherical stability of oscillating gas bubbles. Phys Fluids 11(6):1309

12. Jamialahmadi M, Zehtaban MR, Müller-Steinhagen H, Sarrafi A, Smith JM (2001) Study of bubble formation under constant flow conditions. Chem Eng Res Des 79(5):523–532

13. Das AK, Das PK, Saha P (2011) Formation of bubbles at submerged orifices—experimental investigation and theoretical prediction. Exp Therm Fluid Sci 35(4):618–627

14. Fritz W (1935) Berechnung des maximal volume von dampfblasen. Phys Z 36:379–388

15. Terasaka K, Tsuge H (1991) Bubble formation at a single orifice non-newtonian liquids. Chem Eng Sci 46(1):85–93

16. Badam VK, Buwa V, Durst F (2007) Experimental investigations of regimes of bubble formation on submerged orifices under constant flow condition. Can J Chem Eng 85(June):257–267

17. Fan W, Jiang S, Zhu C, Ma Y, Li H (2008) Study on bubble formation in non-Newtonian fluids by laser image technique. Opt Laser Technol 40(2):389–393

18. Di Bari S, Robinson AJ (2013) Experimental study of gas injected bubble growth from submerged orifices. Exp Therm Fluid Sci 44:124–137

19. Hanafizadeh P, Eshraghi J, Kosari E, Ahmed WH (2015) The effect of gas properties on bubble formation, growth and detachment. Part Sci Technol 6351:150407162559008

20. Kulkarni AA, Joshi JB (2005) Bubble formation and bubble rise velocity in gas-liquid systems: a review. Ind Eng Chem Res 44:5873–5931

21. Corchero G, Medina A, Higuera FJ (2006) Effect of wetting conditions and flow rate on bubble formation at orifices submerged in water. Colloids Surfaces A Physicochem Eng Asp 290(1–3):41–49

22. Vafaei S, Wen D (2010) Bubble formation on a submerged micronozzle. J Colloid Interface Sci 343(1):291–297

23. Eral HB, 'T Mannetje DJCM, Oh JM (2013) Contact angle hysteresis: a review of fundamentals and applications. Colloid Polym Sci 291(2):247–260

24. Hanafizadeh P, Ghanbarzadeh S, Saidi MH (2011) Visual technique for detection of gas–liquid two-phase flow regime in the airlift pump. J Pet Sci Eng 75(3–4):327–335

25. Keshock EG, Siegel R (1964) Forces acting on bubbles in nucleate boiling under normal and reduced gravity conditions. NASA Tech. Note TN D-2299, no. August, p 28

26. Morrison F (2013) Data correlation for drag coefficient for sphere. Michigan Technol. Univ. Houghton, MI, vol 6, pp 1–2

27. Duhar G, Colin C (2006) Dynamics of bubble growth and detachment in a viscous shear flow. Phys Fluids 18(7):77101